Monotonically decreasing size distributions for one-dimensional Ga rows on Si(100)

M. A. Albao,[1] M. M. R. Evans,[2] J. Nogami,[3] D. Zorn,[4] M. S. Gordon,[4] and J. W. Evans[5]
[1]*Ames Laboratory, USDOE, and Department of Physics and Astronomy, Iowa State University, Ames, Iowa 50011, USA*
[2]*Department of Physics and Astronomy, University of Wisconsin–Eau Claire, Eau Claire, Wisconsin 54702, USA*
[3]*Department of Materials Science and Engineering, University of Toronto, Toronto, Ontario, Canada M5S 3E4*
[4]*Ames Laboratory, USDOE, and Department of Chemistry, Iowa State University, Ames, Iowa 50011, USA*
[5]*Ames Laboratory, USDOE, and Department of Mathematics, Iowa State University, Ames, Iowa 50011, USA*
(Received 4 November 2004; revised manuscript received 2 February 2005; published 8 July 2005)

Deposition at room temperature of Ga on Si(100) produces single-atom-wide metal rows orthogonal to the Si-dimer rows. Detailed analysis using scanning tunneling microscopy reveals a monotonically decreasing size (i.e., length) distribution for these rows. This is unexpected for homogeneous nucleation without desorption, conditions which are operative in this system. Kinetic Monte Carlo simulation of an appropriate atomistic model indicates that this behavior is primarily a consequence of the feature that the capture of diffusing atoms is greatly inhibited in the Ga/Si(100) system. The modeling also determines activation barriers for anisotropic terrace diffusion, and recovers the experimental distribution of metal rows. In addition, we analyze a variety of other generic deposition models and determine that the propensity for a large population of small islands in general reflects an enhanced nucleation rate relative to the aggregation rate.

DOI: 10.1103/PhysRevB.72.035426 PACS number(s): 68.55.Ac, 68.37.Ef, 68.55.Jk, 81.15.Aa

I. INTRODUCTION

Deposition of atoms on perfect low-index single-crystal surfaces typically leads to diffusion-mediated organization into islands.[1–3] These islands could be one, two, or three dimensional, compact or dendritic or fractal, coherent or dislocated, depending on such factors as the surface or substrate symmetry, the lattice mismatch between overlayer and substrate, and the efficiency of island shape relaxation dynamics. Availability of atomic-resolution scanning tunneling microscopy (STM) images allows detailed comparison between measurements of island density, size distributions, and structure, and predictions of atomistic models of growth.[1–3] Ideally, such modeling provides insight into the key atomistic processes controlling growth. This approach can be particularly effective if judiciously selected variations of the model are simulated to identify the effect of specific processes. Ideally, modeling also allows accurate determination of the activation barriers for these processes. These barriers may not be readily or precisely accessible from electronic structure calculations. Ultimately, insight derived from this combination of experiment and modeling can lead to better control of nanostructures formed during deposition.

In this paper, we report on the room temperature growth of Ga on Si(100) for which scanning tunneling microscopy studies reveal that the metal islands formed during deposition are single-atom-wide one-dimensional atomic rows.[4–7] Similar behavior applies for other group III metals In, Al,[4–7] and Tl,[8] and for the group IV metals Sn and Pb.[9] Precise data for the Ga island size distribution reveal an unconventional monotonically decreasing form. (Size distribution data showing the same form were also taken for Sn and In, but will not be included here.) This form will be recovered from simulations of an atomistic model incorporating the key features of adatom interactions in this system: sites adjacent to metal rows are energetically unfavorable, and adatoms aggregate only at the ends of rows.

Several features make group III metals on Si(100) an ideal class of systems for study. First, multilayer growth is strictly absent in the low-coverage regime $\theta < 0.5$ monolayer (ML), so modeling need not address population of higher layers. Second, STM studies[4–7] as well as electronic structure calculations[10] provide insight into the adatom interactions mediating the local atomic arrangement of adatoms into islands or rows on the surface. Specifically, metal adatoms have a strong tendency to form dimers which constitute the minimum stable unit on the surface, a feature exploited in our modeling. These metal dimers in turn arrange themselves in rows which lie orthogonal to the Si-dimer rows on the clean 2×1 reconstructed Si(100) surface. There is an effective repulsion between metal rows which are directly adjacent. Consequently, such rows must be separated by a minimum distance of $2a$ (shown as A in Fig. 1), where $a=0.384$ nm is the Si unit cell spacing. Diffusing metal adatoms can bond with rows only at the two end sites (shown as B and gray squares in Fig. 1) which are highly reactive due to the presence of dangling bond states. Those sites adjacent to a metal row are energetically unfavorable (shown as C and crossed squares in Fig. 1) presumably since half of the Si atoms associated with that row are already bonded to metal atoms. Thus, aggregation of diffusing adatoms with the metal rows is highly restricted. These and other features shown in the schematic, Fig. 1, are consistent with the STM data and analysis immediately following. They also serve to illustrate the essential ingredients of our atomistic model, described in more detail in Sec. III.

Experimental results are first presented in Sec. II. Then, we describe our atomistic model in Sec. III, and compare predictions of this model obtained from kinetic Monte Carlo simulation with experimental observations in Sec. IV. Then, in Sec. V, we present a more detailed analysis and elucidation of the dependence of island nucleation behavior on different specific aspects of this model. Next, in Sec. VI, we review behavior of models which have some features in

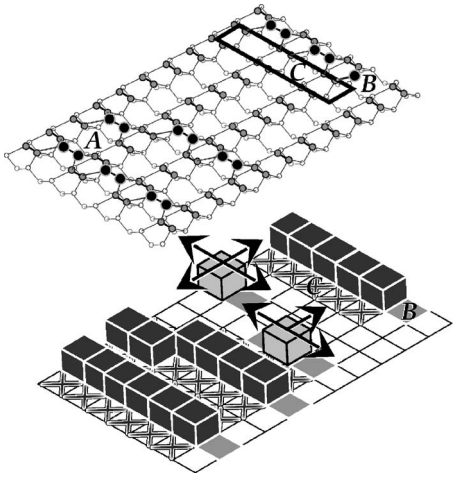

FIG. 1. (Top) The atomic structure of rows of Ga (dark circles) on Si(100) which run orthogonal to the rows of Si dimers (gray circles). Ga rows with the minimum separation are indicated by *A*. Blocked sites are indicated by *C*. Aggregation sites are indicated by gray squares and *B*. (Bottom) Lattice-gas model reproducing the section of the surface shown in (a). Ga atoms frozen in rows are dark cubes. Diffusing Ga adatoms are gray cubes. Gray squares and B indicate aggregation sites. Crossed squares and *C* indicate blocked sites.

common with our model for Ga on Si(100). In addition, in Sec. VI and the Appendix, we provide a comprehensive analysis of a broader class of models to reveal that enhanced nucleation relative to aggregation in general boosts the population of small islands and can produce monotonically decreasing island size distributions. Finally, our findings are summarized in Sec. VII.

II. EXPERIMENTAL RESULTS AND ANALYSIS

A typical STM image of Ga rows formed by deposition of 0.09 monolayer of Ga on Si(100) at room temperature with flux $F=10^{-3}$ ML/s is shown in Fig. 2. In order to appropriately analyze such experimental data for the metal island or row size distribution, we first recall a central observation from recent analyses in nucleation theory. For island formation during deposition, simulation[11,12] and theory[12,13] indicate that the density (per site) of islands of size s (measured in atoms) satisfies the scaling relation

$$N_s \approx N_{isl}\frac{f(s/\langle s\rangle)}{\langle s\rangle} = \theta\frac{f(s/\langle s\rangle)}{\langle s\rangle^2} \qquad (1)$$

Here, $N_{isl}=\theta/\langle s\rangle$ denotes the mean island density (per site), for coverage θ given in ML, and mean island size $\langle s\rangle$. The scaling function $f(x)$ describes the shape of the island size distribution as a function of the scaled island size $x=s/\langle s\rangle$. This function is normalized so that $\int_{x\geq 0} f(x)dx = \int_{x\geq 0} xf(x)dx = 1$, and it usually depends only weakly on coverage, in the low-θ regime. Most commonly, the shape of $f(x)$ versus $x=s/\langle s\rangle$ is monomodal with a well-defined peak around $x=1$. This monomodal form occurs for both homogeneous nucleation[11–13] [expected to dominate in the Ga on Si(100) system], and for heterogeneous nucleation.[14,15] For homogeneous nucleation, the width of the peak in this monomodal distribution decreases (so the population of small islands becomes negligible) with increasing the critical size *i* above which islands are stable.[11,16]

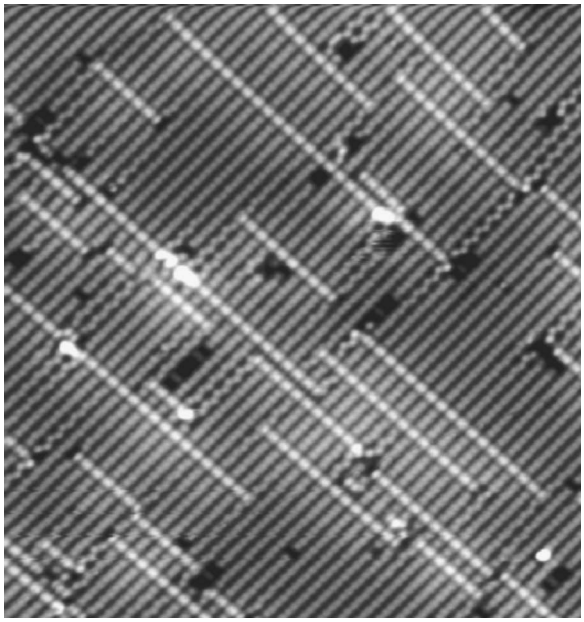

FIG. 2. Filled state STM image $(32.5\times 32.5\ \text{nm})^2$ of Ga rows on Si(100) at 0.09 ML. Ga rows run from upper left to lower right, orthogonal to Si-dimer rows.

Figure 3 shows experimental STM data for $f(x)=N_s\langle s\rangle^2/\theta$ as a function of $x=s/\langle s\rangle$ for six coverages of Ga on Si(100). The scaling behavior is consistent with Eq. (1). Data for each coverage are obtained by measuring the length of rows in 4–12 images corresponding to a total area of $(100\ \text{nm})^2$ to $(400\ \text{nm})^2$. It was assumed that the number of atoms in each row was even, corresponding to complete dimers. Detailed analysis of high-resolution images in fact shows that rows are equally likely to be terminated by a metal dimer or monomer, so the effects of this assumption should average out.[6] Figure 4 shows the average row size (or

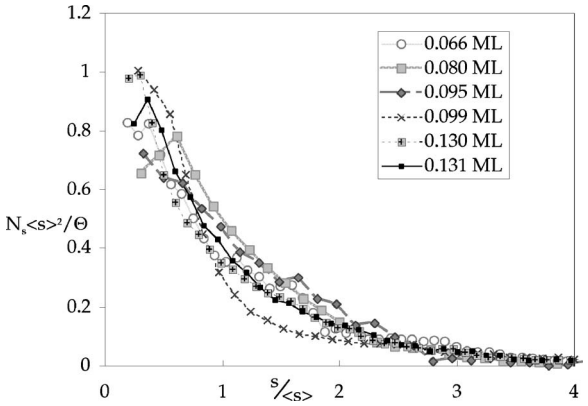

FIG. 3. Experimental results for the scaled island size distribution, $f=N_s\langle s\rangle^2/\theta$, versus $x=s/\langle s\rangle$ for Ga on Si(100) at different metal coverages (given in the legend).

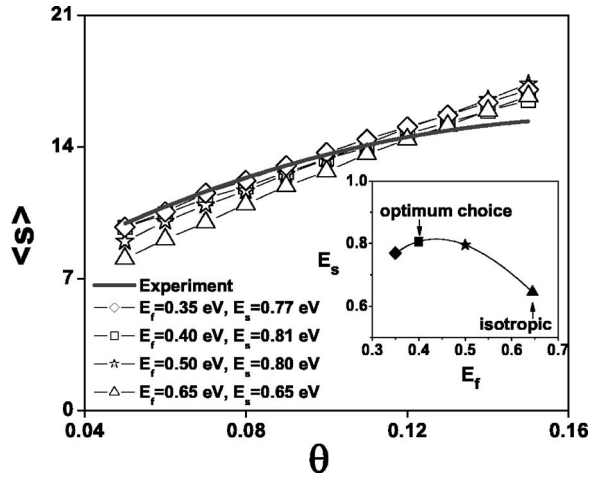

FIG. 4. Average island size, i.e., row length (measured in atoms), versus coverage. The thick black line indicates the experimental data. Open symbols connected by thin lines show the simulation results for various degrees of anisotropy in terrace diffusion (indicated in the legend). These values of diffusion parameters (E_s, E_f), chosen to match $\langle s \rangle$ at around 0.10–0.12 ML, are also displayed in the inset.

length) from the experimental data which increases rather slowly with coverage between 0.05 and 0.15 ML, indicating persistent nucleation of new islands in this regime. As an aside, while there are defects on the surface, their density is always less than 0.01 ML, and is typically around 0.003 ML. Moreover, images of the same area of the surface before and after deposition explicitly demonstrate that nucleation occurs primarily away from defects on the surface.

What is striking about the Ga/Si(100) data is the similar monotonically decreasing island size distribution for all coverages, as shown in Fig. 3. In studies not reported here, we find the same behavior for In and Sn on Si(100). One caveat with this description of the data is that we do not exclude the possibility of a "weak" peak for small x. As is typical for deposition studies, it is difficult to obtain sufficient data to reduce statistical uncertainty to the point of being able to precisely determine such fine features of the size distribution. Irrespective of whether such a weak peak occurs, observed behavior is in marked contrast to that typically observed for homogeneous nucleation, which is operative for group III metals on Si(100), where f is typically monomodal with clear peak around $x=1$.[11] Finally, it should be noted that monotonically decreasing size distributions are produced for deposition models including (i) exchange-mediated nucleation, (ii) incomplete condensation, and (iii) postdeposition nucleation. However, none of these scenarios applies for group III metals on Si(100). Nonetheless, in Sec. VI and the Appendix, we will identify the certain common features of these models and the Ga/Si(100) system which underly the appearance of such size distributions.

III. ATOMISTIC LATTICE-GAS MODEL

In order to gain insight into the origin of this unusual size distribution for Ga/Si(100), we turn to detailed atomistic modeling. Below, we describe the surface by a square lattice of adsorption sites in which metal dimer rows run from left to right. Thus, sites above or below them are energetically unfavorable (as described above) and are treated as being blocked to diffusing adatoms in our modeling (cf. crossed squares in Fig. 1). We assume an Arrhenius form for the rates of adatom hopping, $h=\nu \exp[-E_{\rm act}/(k_B T)]$, for Si surface temperature $T=300$ K. The attempt frequencies are chosen as $\nu=10^{13}$/s, and the activation barriers $E_{\rm act}$ are specified below. Our model includes the following steps (cf. Fig. 1).

(i) Metal atoms are deposited randomly at adsorption sites at rate $F=10^{-3}$ ML/s matching experiment. If the selected site is available, the atom is placed there. If it is occupied by another metal atom, or is blocked (as described above), then the deposited atom is moved to a nearby available site in a way designed to mimic the actual deposition and subsequent diffusional dynamics. Various scenarios are described below.

(ii) If the atom lands on a metal monomer, or on the end of a metal row, it checks the sites to the left or right for availability. (Such sites could be blocked by a neighboring metal row.) If available, it is placed there. If not, see (iv) below.

(iii) If the atom lands at a site which is in the mid-region of a metal row, since sites directly above and below are blocked, it checks sites two lattice constants either above or below for availability. If available, it is placed there, and if not see (iv) below.

(iv) If the site checked in (ii) or (iii) is unavailable, its neighbors are also checked for availability. Again the atom is placed there if available, but if not a more extensive search for an available site is needed. In fact, at least at higher submonolayer coverages, an atom can be deposited far from an available site. Then, it needs to diffuse along one-dimensional (1D) rows of blocked sites parallel to the metal atom rows in order to find a site. We implement this process searching for the nearest available sites in either direction along the row of blocked sites, and then using analytic results for 1D diffusion between traps to suitably select one of these.[17]

(v) Isolated metal adatoms undergo anisotropic diffusion across the surface, hopping to adjacent sites provided these are available (i.e., not occupied or blocked). Rates are different for hopping parallel and orthogonal to metal rows. See below.

(vi) Pairs of diffusing adatoms irreversibly nucleate new islands when they meet on adjacent sites in the same row. Diffusing adatoms are irreversibly captured when they reach sites at the end of metal rows, thus leading to island growth by irreversible aggregation. Irreversible nucleation and growth, usually referred to as critical size $i=1$, also occurs when a deposited atom lands in a site to the left or right of another isolated metal adatom or at the end of a metal row, respectively (site B or gray squares in Fig. 1).

Our kinetic Monte Carlo simulations for this atomistic model are implemented using an efficient Bortz-type algorithm[1] tracking all of the diffusing adatoms.

We now discuss in more detail the characterization of anisotropic terrace diffusion of group III metals on Si(100). Electronic structure analyses of this issue include earlier

plane-wave density functional theory (DFT) calculations using a Car-Parrinello optimization technique.[10] More recently, we have performed *ab initio* calculations using a multiconfiguration self-consistent field molecular orbital–molecular mechanics embedded cluster method,[18] augmented by second-order perturbation theory. For the latter, a cluster of Si surface atoms in the neighborhood of the diffusing atom is treated by high-level *ab initio* methods, and embedded in a much larger cluster of surrounding Si substrate atoms which are treated by a classical molecular mechanics model potential. Indeed, we do find some metal adsorbate structures with a significant multiconfigurational or diradical character which cannot be adequately handled by DFT. However, both DFT and *ab initio* studies indicate that the fast diffusion direction for a group III metal (Al) on Si(100) is orthogonal to the Si-dimer rows, i.e., parallel to the metal rows. Since it is expected that the planned calculations on Ga will provide qualitatively similar predictions to those found for Al, the key finding here guides our parameter choices in the modeling below.

IV. COMPARISON OF MODEL PREDICTIONS WITH EXPERIMENT

A primary constraint on our modeling is to match the mean island size $\langle s \rangle$ (at around 0.1 ML, say), noting that this is equivalent to matching the mean island density, $N_{isl}=\theta/\langle s \rangle$. In fact, we find that $\langle s \rangle$ at 0.10–0.12 ML can be matched for various choices of activation barriers $E_{\mathrm{act}}=E_f$ for fast hopping in a direction parallel to the metal rows, and $E_{\mathrm{act}}=E_s$ for slow hopping in the perpendicular direction. These choices range from isotropic, with $E_f=E_s=0.65$ eV, to strongly anisotropic, as shown in the inset to Fig. 4. In Fig. 4, we further show that all of these choices reasonably match the experimental $\langle s \rangle$ versus θ. However, it could be argued that the strongly anisotropic choice with $E_f=0.40$ eV and $E_s=0.81$ eV is marginally better (with respect to both absolute values of $\langle s \rangle$ and the slow increase with θ). Simulation results showing a typical distribution of metal rows for our model with this anisotropic choice of diffusion parameters are presented in Fig. 5.

More compelling evidence that the strongly anisotropic choice is optimum comes from analysis of the island size distribution. In Fig. 6, we show that the size distribution evolves from a monomodal form for isotropic diffusion (contrasting experiment) to a monotonically decreasing form for strongly anisotropic diffusion with $E_f=0.40$ eV and $E_s=0.81$ eV (consistent with experiment). Finally, for this optimal parameter choice, in Fig. 7, we present comprehensive results for the coverage dependence of the predicted island size distribution which agrees well with experiment. It should be noted that a rather weak peak in the distribution develops for higher coverages, but that this peak corresponds to small sizes, $x \approx 1/4$, in contrast to the behavior for conventional nucleation models where the peak is at $x \approx 1$.

To close this section, we comment briefly on three additional observations from our simulation studies. First, one might regard the large finite barrier E_s to be effectively infinite. However, one unexpected result of our analysis is that

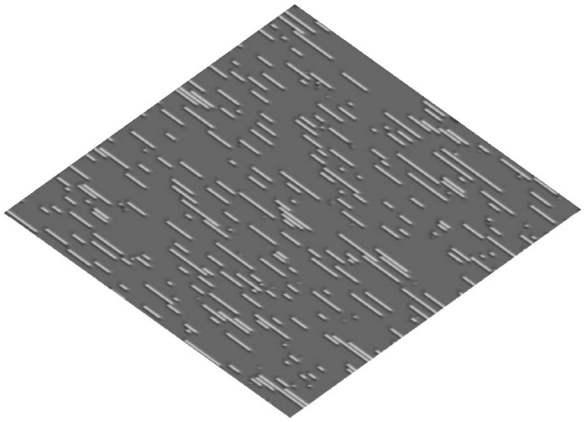

FIG. 5. Simulated configuration of Ga rows on Si(100) in a 70×70 nm^2 region using the optimum parameters for our physical model described in the text.

setting $E_s=\infty$ (for fixed E_f) does significantly increase N_{isl}. Second, another unconventional trend observed in our simulations is that decreasing E_f from 0.5 eV to 0.4 eV (for fixed E_s) does not significantly decrease the island density, as would be expected from conventional nucleation theories.[1,11,19] Both these features are discussed in the following section. Third, it is natural to consider whether the observed features of the island size distribution vary significantly with deposition flux F. In experiment, it is difficult to vary F by many orders of magnitude. Ideally, one would like to significantly decrease F from its already low value of 10^{-3} to explore the regime of larger $\langle s \rangle$. It is straightforward to explore this regime with our simulation model. We find that for $F=10^{-4}$, the size distribution develops a peak, which is still weak but more discernible than for $F=10^{-3}$. However, again this peak occurs for small sizes with x below 1/2, in contrast to the usual behavior for homogeneous nucleation.

V. DEPENDENCE OF NUCLEATION BEHAVIOR ON VARIOUS ASPECTS OF THE ATOMISTIC MODEL

Island nucleation behavior and the form of the size distribution in the Ga/Si(100) system, and in our modeling de-

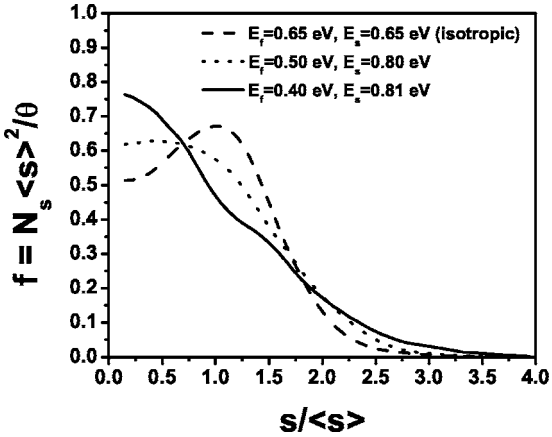

FIG. 6. Simulation results for the scaled island size distribution, $f=N_s\langle s \rangle^2/\theta$, versus $x=s/\langle s \rangle$ for different degrees of diffusional anisotropy (shown).

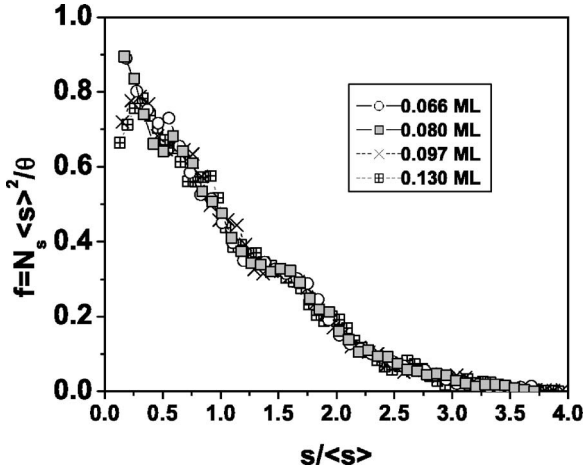

FIG. 7. Simulation results for the scaled island size distribution, $f=N_s\langle s\rangle^2/\theta$, versus $x=s/\langle s\rangle$ using the optimum parameters for our physical model described in the text. Behavior is shown for different metal coverages (given in the legend).

scribed above, are quite distinct from those in more conventional models.[1,11,19] To elucidate these unconventional features, it is instructive to compare behavior for a variety of refinements to the above physical model (PM), all of which retain the same diffusion parameters. The models which we compare here differ from our PM above in the following ways.

(a) Enhanced transport (ET): "blocked" sites no longer restrict diffusion of isolated adatoms, but do still preclude nucleation and aggregation.

(b) Enhanced nucleation (EN): sites above and below islands again block diffusion and aggregation, but now sites above and below an isolated atom become accessible nucleation sites for another diffusing atom (rather than just sites to the left or right as in the PM). In the event of such nucleation, the metal atom pair is reoriented along the designated direction for metal rows.

(c) Enhanced aggregation (EA): again sites above and below islands and atoms are blocked as in the PM, but now we add two additional next-nearest-neighbor aggregation sites at each end of metal row. These are directly above and below the aggregation sites for the PM.

We also consider behavior for a more conventional "point island" (PI) model with the same diffusion parameters as in the above models. In a PI model,[11] each metal island (and adatom) occupies a single site, but carries label to indicate its size. Nucleation or aggregation occurs when diffusing atoms reach any of the four neighbors, after which the size label for the point island is appropriately updated.

First, one might expect that enhanced transport leads to enhanced nucleation and higher island densities, as it becomes easier for diffusing atoms to find each other. Indeed, ET does increase N_{isl} by a factor of three at ~ 0.05 ML compared to the PM. Second, enhanced nucleation could potentially also lead to a significant increase of N_{isl}. However, we find that EN produces only a $\sim$25% increase in N_{isl} relative to the PM. In addition, the monotonically decreasing island size distribution of the PM is preserved for EN. Third, enhanced aggregation would likely reduce the density of diffusing adatoms and thus reduce island nucleation. In fact, EA has a much more dramatic effect than ET or EN, greatly reducing N_{isl} to $\sim$20% of its value in the PM at ~ 0.05 ML. The behavior of N_{isl} versus θ changes very little if one adds nucleation sites to this EA model. Furthermore, behavior for EA is almost identical to that for the point island model with the same diffusion parameters. For both EA and PI models, a conventional monomodal island size distribution is observed. All of these results for N_{isl} are presented in Table I. Thus, in conclusion, from these carefully selected tailored studies, it is clear that a primary cause of unconventional behavior in the Ga/Si(100) system and in our physical model is the highly restricted nature of aggregation compared to a more conventional nucleation model.

TABLE I. Comparison of the values of the island density, N_{isl}, and the isolated adatom density, $n=N_1$, at a Ga coverage of 0.04 ML for various models described in the text: PM, physical model; ET, enhanced transport; EN, enhanced nucleation; EA, enhanced aggregation; PI, point island model. Anisotropic diffusion parameters were chosen in all models as $(E_f,E_s)=(0.40\text{ eV},0.81\text{ eV})$.

	PM	ET	EN	EA	PI	
N_{isl}	0.44	1.23	0.60	0.092	0.105	$\times 10^{-2}$/site
N_1	4.8	17.2	3.7	0.15	0.10	$\times 10^{-4}$/site

Except for the very initial stage of deposition, a quasi-steady-state[1,11,19] is typically operative, where there is a rough balance between gain of isolated adatoms due to deposition and loss due to aggregation or nucleation. Thus, greatly restricting aggregation should significantly boost the density of isolated adatoms. This feature can be checked easily and directly with simulation (but not with experiment). We simply monitor the density of isolated adatoms, $n=N_1$, during deposition in the PM, and compare its value with that of a conventional or point island model with the same diffusion parameters. Indeed, we find that n is greatly enhanced in the PM relative to the PI (up to $\sim 5\times 10^{-4}$/site in the PM compared with $\sim 10^{-5}$/site in the PI, for coverages between 0.01 and 0.1 ML). See Table I. This enhanced adatom density produces the unusually persistent nucleation observed in experiment (and in the PM) compared to conventional systems where nucleation is strongly quenched once islands have achieved a significant size.[1,11,19] The enhanced adatom density and restricted aggregation must also underlie the deviation of expected variation of the island density with the barrier for fast diffusion.

Finally, we briefly comment on the effect of large finite E_s versus infinite E_s. Normally, values for activation barriers as high as $E_s \approx 0.8$ eV at 300 K would make the associated hopping process insignificant. However, in the Ga/Si(100) system, because the isolated adatom density is high and because even a small amount of diffusion in the slow direction provides a pathway to otherwise inaccessible aggregation sites in adjacent rows, this effect is significant.

VI. DISCUSSION AND COMPARISON WITH OTHER MODELS

First, we should also mention that there exist several previous studies of systems which form 1D islands at lower T.

One example involves deposition of metal atoms on anisotropic fcc(110) surfaces.[20,21] Here, strong bonding occurs only at the end of the metal rows which are the dominant aggregation sites for lower T. However, weak bonding occurs on the sides, so aggregation is not inhibited as for Ga/Si(100). Another example of 1D island formation is provided by Si(100) homoepitaxy at low T.[22] However, the size distribution for these systems exhibits a conventional monomodal form rather than a monotonically decreasing form.[11,23,24]

Next, it is appropriate to note that a few previous studies have examined models or systems which incorporate one feature reminiscent of Ga/Si(100) and of our physical model. Specifically, Kandel[25] considered models for island formation during deposition where there is an additional barrier for hopping processes leading to island nucleation and aggregation (relative to the barrier for terrace diffusion). In these cases, the effect of restricted nucleation is more than compensated for by restricted aggregation which leads to a greatly enhanced isolated adatom density, which in turn leads to enhanced nucleation and island densities. One realization of this type of behavior was recently discovered in metal(111) homoepitaxy at lower T where substrate-mediated adatom-adatom interactions include a repulsive ring inhibiting the approach of adatoms to other adatoms or islands.[26] In these systems, N_{isl} is much higher than would be predicted by conventional nucleation theories.[27] The same can be said for the Ga/Si(100) system, as noted above. However, in the metal(111) systems, the island size distribution at low T does not have a monotonically decreasing form.[28]

Finally, it should be noted that monotonically decreasing island size distributions have been observed in models for (i) nucleation mediated by irreversible exchange of single adatoms with the substrate (a process sometimes described as having a critical size $i=0$);[29,30] (ii) nucleation under conditions of strongly incomplete condensation (i.e., deposition when desorption is active),[31,32] and which is described by Avrami-type adsorption kinetics;[32] and (iii) postdeposition nucleation for critical size $i=1$.[33] There has, however, been no previous comprehensive analysis of these models, or comparison with more traditional models, to determine whether there is some generic feature producing monotonically decreasing size distributions (or, more generally, producing a higher population of smaller islands). In the Appendix, we have performed such an analysis using rate equations to assess the relative magnitudes of the nucleation and aggregation rates in these various models. The conclusion is that unusually enhanced nucleation relative to aggregation is seen to produce monomodal size distributions in all the above models. For our model of Ga deposition on Si(100), the same principle seems to apply in that greatly restricted aggregation leads to relatively predominant and persistent nucleation.

VII. SUMMARY

In conclusion, the unusual organization into single-atom-wide atomic rows of group III metals deposited onto Si(100) is now well recognized based on several previous STM studies. However, detailed analysis of these adlayers was lacking in previous studies. Such an analysis was performed here to reveal an unexpected monotonically decreasing form for the island size distribution. This observation was combined with atomistic modeling to provide detailed insight into which aspects of the underlying atomistic processes favor the development of such a distribution. A key factor is inhibited aggregation, resulting from the feature that sites at the sides of metal adatom rows are energetically unfavorable for the diffusing metal adatoms, so these adatoms can attach only at the ends of rows. This leads to unusually enhanced nucleation relative to aggregation, a characteristic shown to exist in other models exhibiting monotonically decreasing size distributions.

ACKNOWLEDGMENTS

We thank Maozhi Li for discussions on the island size distribution in metal(110) homoepitaxy. The experimental work was carried out by M.M.R. and J.N. at the University of Wisconsin–Milwaukee with partial support from the Laboratory for Surface Studies. J.N. acknowledges support from the NSF under the Award No. DMR-0305472. M.A.A., D.Z., M.S.G., and J.W.E. were supported for this work by the Division of Chemical Sciences, and by the SciDAC Computational Chemistry program of the U.S. Department of Energy (USDOE) Basic Energy Sciences. Their work was performed at Ames Laboratory, which is operated for the USDOE by Iowa State University under Contract No. W-7405-ENG-82.

APPENDIX: CORRELATION BETWEEN NUCLEATION BEHAVIOR AND ISLAND SIZE DISTRIBUTION SHAPE

The form of the island size distribution in deposition systems should be sensitive to nucleation behavior. In particular, a tendency towards monotonically decreasing (rather than monomodal) size distributions should be favored by an enhanced nucleation rate relative to the aggregation rate, and by increased persistence of nucleation. This follows since enhanced nucleation will produce more new small islands, thus boosting the relative population of small islands. The behavior of the nucleation rate has received relatively little attention, so here we provide a comparison for various models.

Below, we consider four classes of models for island formation during deposition. All models include random deposition at rate F (with deposition initiated on an empty surface at time $t=0$), and isotropic surface diffusion of isolated adsorbed atoms (adatoms) with hop rate h. Island (diffusing adatom) densities are denoted by N_{isl} (n). For all cases, the rate of aggregation of diffusing atoms with islands is given by $K_{agg}=\sigma_{av}hnN_{isl}$, where σ_{av} is the mean "capture number" for the islands. In the following discussion of the population of small islands for these models, "small" should be interpreted as relative to the average island size. We now provide an explicit description of the four models, and in particular of the island nucleation rate.

TABLE II. Comparison of behavior in various deposition models: $i \geqslant 1$ denotes models with no desorption and homogeneous nucleation with critical size i; $i=0$ denotes a model with exchange-mediated nucleation in the regime of rapid exchange; $d>0$ denotes a model with desorption and homogeneous nucleation with $i=1$ in the regime of rapid desorption. Also "tr" denotes transient regime, and "ss" the steady-state regime, with $*$ denoting the crossover point. K_{nuc} (K_{agg}) denotes nucleation (aggregation) rates. For simplicity, we neglect factors involving E_i, or the capture numbers σ_i or σ_{av}. Approximate forms are given for the steady-state coverage dependence, except for $d>0$ where it is ignored.

	n(tr)	N_{isl}(tr)	Ft^*	K_{nuc}^*/F	K_{agg}^*/F	n(ss)	N_{isl}(ss)
$i>1$	θ	$\theta^{i+2}(h/F)$	$(h/F)^{-2/(i+3)}$	$(h/F)^{-(i-1)/(i+3)} \ll 1$	1	$(h/F)^{-1}N_{isl}^{-1}$	$\theta^{1/(i+2)}(h/F)^{-i/(i+2)}$
$i=1$	θ	$\theta^3(h/F)$	$(h/F)^{-1/2}$	1	1	$(h/F)^{-1}N_{isl}^{-1}$	$\theta^{1/3}(h/F)^{1/3}$
$i=0$	θ	$\sigma_0\theta^2(h/F)$	$(\sigma_0)^{-1}(h/F)^{-1}$	1	$(\sigma_0)^{-2}(h/F)^{-1} \ll 1$	$(\sigma_0)^{-1}(h/F)$	θ
$i=0$ cont.			σ_0	1	1	$(h/F)^{-1}N_{isl}^{-1}$	$(\sigma_0)^{1/2}\theta^{1/2}$
$d>0$	θ	$\theta^3(h/F)$	$(d/F)^{-1}$	$(h/F)(d/F)^{-2}<1$	$(h/F)^2(d/F)^{-4} \ll 1$	$(d/F)^{-1}$	$(h/F)^{1/3}(d/F)^{-1}$

(i) Complete condensation (no desorption) and homogeneous nucleation with critical size $i>1$.[19] The nucleation rate satisfies $K_{nuc}=\sigma_i h n N_i$, where $N_i \approx c_i \exp[-E_i/(k_BT)]n^i$ is the density of critical clusters of i atoms, $E_i<0$ is the associated binding energy, and σ_i is the associated capture number. Here, the island size distribution has a sharp monomodal form with negligible population of small islands.[11,16]

(ii) Complete condensation in the special case of irreversible aggregation ($i=1$).[11,12] The nucleation rate is given by $K_{nuc}=\sigma_1 h n^2$. Here, the island size distribution has a monomodal form with significant population of small islands.[11,12]

(iii) Incomplete condensation where desorption of adatoms now occurs with a "significant" rate $d>0$.[31,32] The above expressions in (i) and (ii) for K_{nuc} still apply for homogeneous nucleation. We just consider the case $i=1$ where there are the two key characteristic lengths: the diffusion length over the lifetime of an adatom before desorption, $L_{des}=(h/d)^{1/2}$, and the typical island separation in the absence of desorption, $L_{isl}(d=0)=(h/F)^{1/6}$. Significant desorption means that $L_{des} \ll L_{isl}(d=0)$. Here, the island size distribution has a monotonically decreasing form with many small islands.[32]

(iv) Heterogeneous nucleation by exchange of deposited adatoms with substrate atoms (so-called $i=0$).[29,30] Here, a single exchanged atom forms a stable nucleus for island growth. The nucleation rate satisfies $K_{nuc}=h_{ex}n=h\sigma_0 n$, where $h_{ex}=h\sigma_0$ is the exchange rate. Previous studies have considered the regime of rapid exchange which we define precisely as $\sigma_0 \approx (h/F)^{-\alpha}$, where $0 \leqslant \alpha < 1/2$. In this regime, the island size distribution has a monotonically decreasing form with many small islands.[29,30]

Analysis of the rate equations for these models reveals an initial "transient" regime for $t \leqslant t^*$ where the adatom density, $n \approx Ft$, increases from its initial zero value due to deposition, followed by a steady-state regime where the gain in adatom density due to deposition is roughly balanced by the loss due to either nucleation or aggregation. Table II summarizes the behavior of n and N_{isl} for the above models in the transient (tr) and steady-state (ss) regimes, as well as the behavior of K_{nuc} and K_{agg} at crossover ($*$) when $t \approx t^*$. Note that for $i=0$, the steady-state regime has two subregimes, the first for $(\sigma_0)^{-1}(h/F)^{-1} < Ft < \sigma_0$ where K_{nuc} dominates K_{agg}, and the second for $\sigma_0 < Ft$ where the opposite applies. Below θ denotes the total surface coverage which equals Ft in all models without desorption. For $d>0$, one has $\theta \approx Ft$ only in the transient regime.

Examination of Table II reveals that monomodal island size distributions with negligible population of small islands for $i>1$ correspond to $K_{nuc}^* \ll K_{agg}^*$; monomodal distributions with significant population of small islands for $i=1$ correspond to $K_{nuc}^* \approx K_{agg}^*$; and monotonically decreasing distributions with a dominant population of small islands for $i=0$ and $d>0$[34] correspond to $K_{nuc}^* \gg K_{agg}^*$. More detailed analysis also reveals that nucleation is more persistent (i.e., K_{nuc} decreases more slowly in the steady-state regime) for $i=0$ and $d>0$ than in the other cases.

Finally, we comment on postdeposition island formation where a random initial distribution of adatoms with coverage θ hops and aggregates into islands with nucleation determined by a prescribed critical size.[33] The mean island density scales like $N_{isl} \sim \theta^{1+z}$, as $\theta \to 0$, where $z=0$ for $i=1$, $z=0.24$ for $i=2$, and $z=0.65$ for $i=3$. Larger z means fewer islands, and thus less nucleation relative to aggregation. Correspondingly, the island size distribution changes from monotonically decreasing for $i=1$ (where $z=0$ means maximal nucleation), to monomodal for $i>1$ where the population of small islands diminishes for increasing i.

[1] T. Michely and J. Krug, *Islands, Mounds, and Atoms* (Springer, Berlin, 2003).

[2] A. Pimpinelli and J. Villain, *Physics of Crystal Growth* (Cambridge University Press, Cambridge, U.K., 1998).

[3] Z. Y. Zhang and M. G. Lagally, Science **276**, 377 (1997).

[4] J. Nogami, S.-I. Park, and C. F. Quate, Appl. Phys. Lett. **53**, 2086 (1988).

[5] J. Nogami, in *Atomic and Molecular Wires*, edited by C. Joachim and S. Roth (Kluwer, Dordrecht, 1997), Vol. 341, p. 11.

[6] M. M. R. Evans and J. Nogami, Phys. Rev. B **59**, 7644 (1999).

[7] J. Nogami and M. M. R. Evans, Surf. Rev. Lett. **6**, 1067 (1999).
[8] A. A. Saranin, A. V. Zotov, V. G. Kotlyar, I. A. Kuyanov, T. V. Kasyanova, A. Nishida, M. Nishida, Y. Murata, H. Okado, M. Katayama, and K. Oura, Phys. Rev. B **71**, 035312 (2005).
[9] H. Itoh, H. Tanabe, D. Winau, A. K. Schmid, and T. Ichinokawa, J. Vac. Sci. Technol. B **12**, 2086 (1994).
[10] G. Brocks, P. J. Kelly, and R. Car, Phys. Rev. Lett. **70**, 2786 (1993).
[11] M. C. Bartelt and J. W. Evans, Phys. Rev. B **46**, 12675 (1992); Surf. Sci. **298**, 421 (1993);J. W. Evans and M. C. Bartelt, J. Vac. Sci. Technol. A **12**, 1800 (1994).
[12] M. C. Bartelt and J. W. Evans, Phys. Rev. B **54**, R17359 (1996);J. W. Evans and M. C. Bartelt, *ibid.* **66**, 235410 (2002).
[13] D. D. Vvedensky, Phys. Rev. B **62**, 15435 (2000);P. A. Mulheran, and D. A. Robbie, Europhys. Lett. **49**, 617 (2000);J. G. Amar, M. N. Popescu, and F. Family, Phys. Rev. Lett. **86**, 3092 (2001).
[14] P. A. Mulheran and J. A. Blackman, Philos. Mag. Lett. **72**, 55 (1995).
[15] V. Fournee, A. R. Ross, T. A. Lograsso, J. W. Evans, and P. A. Thiel, Surf. Sci. **537**, 5 (2003).
[16] J. G. Amar and F. Family, Phys. Rev. Lett. **74**, 2066 (1995);C. Ratsch, P. Smilauer, A. Zangwill, and D. D. Vvedensky, Surf. Sci. **329**, L599 (1995).
[17] For a 1D random walk between two traps, the probability of trapping at either is inversely proportional to the distance to the trap (Refs. 1 and 2). Although diffusion of adatoms along rows of blocked sites to the nearest available site is not strictly a 1D problem, we use this simple formula to determine the final location of the atom (with "negligible error" for our application).
[18] C. H. Choi and M. S. Gordon, in *Computational Materials Chemistry*, edited by L. A. Curtiss and M. S. Gordon (Kluwer, Dordrecht, 2004), p. 125.
[19] J. A. Venables, Philos. Mag. **27**, 697 (1973).
[20] Y. Li, M. C. Bartelt, J. W. Evans, N. Waechli, E. Kamshoff, and K. Kern, Phys. Rev. B **56**, 12539 (1997).
[21] R. Ferrando, F. Hontinfinde, and A. C. Levi, Phys. Rev. B **56**, R4406 (1997).
[22] Y. W. Mo, J. Kleiner, M. B. Webb, and M. G. Lagally, Phys. Rev. Lett. **66**, 1998 (1991).
[23] M. C. Bartelt and J. W. Evans, Europhys. Lett. **21**, 99 (1993).
[24] Maozhi Li (private communication).
[25] D. Kandel, Phys. Rev. Lett. **78**, 499 (1997).
[26] J. V. Barth, H. Brune, B. Fischer, J. Weckesser, and K. Kern, Phys. Rev. Lett. **84**, 1732 (2000).
[27] K. A. Fichthorn and M. Scheffler, Phys. Rev. Lett. **84**, 5371 (2000);A. Bogicevic, S. Ovesson, P. Hyldgaard, B. I. Lundqvist, H. Brune, and D. R. Jennison, *ibid.* **85**, 1910 (2000);S. Ovesson, *ibid.* **88**, 116102 (2002).
[28] K. A. Fichthorn, M. L. Merrick, and M. Scheffler, Phys. Rev. B **68**, 041404(R) (2003).
[29] D. D. Chambliss and K. E. Johnson, Phys. Rev. B **50**, 5012 (1994).
[30] A. Zangwill and E. Kaxiras, Surf. Sci. **326**, L483 (1995).
[31] P. Jensen, H. Larralde, and A. Pimpinelli, Phys. Rev. B **55**, 2556 (1997).
[32] P. A. Mulheran and D. A. Robbie, Philos. Mag. Lett. **78**, 247 (1998).
[33] J. Li, A. G. Rojo, and L. M. Sander, Phys. Rev. Lett. **78**, 1747 (1997).
[34] For $d>0$, significant desorption, where $L_{des} \ll L_{isl}(d=0)$, implies that $d/h \gg (h/F)^{-1/3}$ or $d/F \gg (h/F)^{2/3}$. This in turn implies that $(h/F)(d/F)^{-1} < (h/F)^{-1/3} < 1$, which is used in our analysis for Table II.